International Journal of Applied Earth Observations and Geoinformation 117 (2023) 103192

Contents lists available at ScienceDirect

International Journal of Applied Earth Observations and Geoinformation

journal homepage: www.elsevier.com/locate/jag

Continual expansion of *Spartina alterniflora* in the temperate and subtropical coastal zones of China during 1985–2020

Xi Zhang [a], Xiangming Xiao [b,*], Xinxin Wang [a], Xiao Xu [c], Shiyun Qiu [c], Lianghao Pan [a,d], Jun Ma [a], Ruiting Ju [a], Jihua Wu [e], Bo Li [c,*]

[a] *Ministry of Education Key Laboratory of Biodiversity Science and Ecological Engineering, National Observations and Research Station for Wetland Ecosystems of the Yangtze Estuary, Institute of Biodiversity Science and Institute of Eco-Chongming, School of Life Sciences, Fudan University, Shanghai 200438, China*
[b] *Department of Microbiology and Plant Biology, Center for Earth Observation and Modeling, University of Oklahoma, Norman, OK 73019, USA*
[c] *Yunnan Key Laboratory of Plant Reproductive Adaptation and Evolutionary Ecology and Centre for Invasion Biology, Institute of Biodiversity, School of Ecology and Environmental Science, Yunnan University, Kunming 650504, Yunnan, China*
[d] *Guangxi Key Lab of Mangrove Conservation and Utilization, Guangxi Mangrove Research Center, Guangxi Academy of Sciences, Beihai 536000, China*
[e] *State Key Laboratory of Grassland Agro-Ecosystems, College of Ecology, Lanzhou University, Lanzhou 730000, China*

ARTICLE INFO

Keywords:
Saltmarshes
Spartina alterniflora
Pixel- and phenology-based algorithm
Spatiotemporal dynamics
Drivers

ABSTRACT

Biological invasions are considerably altering ecosystem structure and functions, especially in coastal ecosystems that are subject to intensive anthropogenic disturbances. *Spartina alterniflora* has been recognized as the most serious invasive species in coastal China, which has received considerable attention from the government and the public. There is urgent need to control this invasive species at regional and national scales, but such efforts were impeded by lack of time-series data of *Spartina* spread. Here, we assessed the pixel- and phenology-based algorithm for mapping *Spartina* saltmarshes, and applied this algorithm to generate annual *Spartina* saltmarsh maps (30-m spatial resolution) from 1985 to 2020 by using time series Landsat 5/7/8 images. The resulting maps suggest that *Spartina* has been expanding since 1990 in coastal China, with three noticeable phases (rapid, moderate, and rapid). Along the latitudinal gradient, *Spartina* exhibited a longer invasion history and more frequent changes at low latitudes. Although human interventions caused the decline of *Spartina* in certain areas, rapid natural spread was primarily responsible for its extensive and continual invasion. These results provide insights for efficiently managing this invasive species, enhancing the conservation of coastal wetlands, and promoting the sustainability of coastal wetlands.

1. Introduction

Invasive plant species threaten native ecosystems and biodiversity over islands and coastal regions (Dawson et al., 2017). The perennial grass *Spartina alterniflora* (hereafter, *Spartina*), a species native to Atlantic coastal America, has invaded wetlands worldwide from equatorial regions to coastal Scotland (~57°N) over the past two centuries (Civille et al., 2005). *Spartina* was first introduced to China in 1979 for the purposes of seashore stabilization, tideland reclamation, and soil amelioration (Chung, 2006; Li et al., 2009). Owing to its great adaptability and high reproductive capacity, introduced *Spartina* has extensively invaded coastal China (Chen et al., 2020; Liu et al., 2018; Zuo et al., 2012) and imposed serious negative impacts on coastal wetlands (Xie et al., 2019). In early 2003, the State Environmental Protection Administration of China listed *Spartina* as one of the first 16 invasive species. Some local governments recognized the serious problems caused by overwhelming *Spartina* invasion and initiated several projects to control its expansion at local scale (Li et al., 2022; Yan et al., 2021). Over the recent years, the Chinese government has also recognized the importance and urgency of further controlling *Spartina* expansion and restore native coastal wetlands at regional and national scales (Li et al., 2022). These efforts require data and information on both the present and historical distributions of *Spartina* saltmarshes. Continual records of *Spartina* encroachment at high spatial resolution can help better understand the invasion processes and develop effective management practices, however, such datasets are not readily available for most coastal zones of China.

Over the recent years, satellite remote sensing has been widely used

* Corresponding authors.
E-mail addresses: xiangming.xiao@ou.edu, bool@ynu.edu.cn (B. Li).

https://doi.org/10.1016/j.jag.2023.103192
Received 10 October 2022; Received in revised form 28 December 2022; Accepted 11 January 2023
Available online 19 January 2023

to classify and map *Spartina* saltmarshes, and many researchers have used free satellite images such as Landsat images (Mao et al., 2019; Sun et al., 2016; Wang et al., 2021a; Zeng et al., 2022). We did a literature review on the image data, in-situ reference data, and classification methods used in remote sensing of *Spartina* saltmarshes (Zhang et al., 2020b). To date, the *Spartina* saltmarsh maps have been mostly produced either for specific year(s) or certain small region(s). The data and information about the spatiotemporal changes of *Spartina* saltmarshes at the temporal resolution of one year or multi-year and at large spatial scale remain limited. In an effort to address this data and information gap, our previous work developed and reported a pixel- and phenology-based mapping algorithm, and the results showed that the algorithm performed well when tracking the expansion and removal of *Spartina* during 1995–2018 on Chongming island, Shanghai (Zhang et al., 2020b). There is a need to apply and assess this pixel- and phenology-based algorithm to identify and map *Spartina* saltmarshes on large scale.

The invasion, expansion, and reduction of *Spartina* saltmarshes in coastal China are associated with several factors, and comprehensively understanding these factors is important for understanding the biology and ecology of invasive species. On the one hand, many environmental factors have been found to affect the *Spartina* invasions. For example, inundation and salinity are two critical environmental factors that affect the growth potential and spatial distribution of *Spartina* along the intertidal elevation gradient (Li et al., 2018; Xie et al., 2021). On the other hand, human activities exert both positive and negative effects on the spatial distribution of *Spartina* saltmarshes. The intentional introductions of *Spartina* occurred in many coastal provinces of China during the 1980s and 1990s, which initiated *Spartina* expansion (Ren et al., 2021a). Recently, land reclamation and geomorphological modifications driven by human activities have promoted the spread of *Spartina* (Kirwan and Megonigal, 2013; Xie et al., 2021; Zhu et al., 2022). Human-induced land use and land cover changes for economic development (e.g., aquaculture and agriculture) as well as ecological engineering projects for restoring coastal wetlands have largely reduced the extent of *Spartina* saltmarshes in certain areas (Mao et al., 2019). Although some attempts have been made to investigate the relationships between *Spartina* expansion and potential driving factors (Zhang et al., 2020a; Zhu et al., 2019), previous studies have mostly focused on how environmental factors affect *Spartina* saltmarsh dynamics. The roles of past and current human activities in shaping the expansion and contraction of *Spartina* saltmarshes remain largely unexplored.

Here, we focused on three questions: (1) How well does the pixel- and phenology-based algorithm perform when mapping *Spartina* saltmarshes over temperate and subtropical coastal China? (2) How do *Spartina* saltmarshes temporally change at the provincial scale and spatially vary at the pixel scale? (3) What major factors are responsible for the changes in *Spartina* saltmarshes? First, based on our previous work on Chongming island, Shanghai, China (Zhang et al., 2020b), we extended the pixel- and phenology-based *Spartina* saltmarsh mapping algorithm to temperate and subtropical coastal China, and generated annual *Spartina* saltmarsh maps from 1985 to 2020. Taking the *Spartina* saltmarsh map produced for 2015 as a reference, we assessed the accuracy of the derived maps. Second, we quantified the spatiotemporal dynamics of *Spartina* saltmarshes at different spatial scales, analyzed the areal changes, and investigated the latitudinal variations. Third, we identified the major factors driving *Spartina* saltmarsh gains and losses and evaluated the effect of human activities. The results from this study could provide more comprehensive and accurate information on the spatiotemporal dynamics of *Spartina* saltmarshes over temperate and subtropical coastal China during 1985–2020, which can be used to support invasion ecology, biodiversity protection, and wetland conservation.

2. Materials and methods

2.1. Study area

The native range of *Spartina* in North America varies from ~27°N to 45°N (Kirwan et al., 2009), and the area invaded by *Spartina* in China ranges from ~20°N to 40°N (Zuo et al., 2012). Our early work studied the phenology of *Spartina* saltmarshes with time series Landsat and Sentinel images along the latitudinal gradient in China and found that the phenological discrepancy of *Spartina* and other native saltmarshes was more discernible in temperate and subtropical zones than in tropical zone (Zhang et al., 2022). The subtropical climate is not a well-defined term but is generally delineated over the latitudinal range between 23.5°N/S and 35°N/S. Previous studies (Gu et al., 2021; Zhang et al., 2017) have reported that more than 90% of *Spartina* saltmarshes are distributed within the temperate and subtropical zones of coastal China. In this study, we therefore chose the coastal zone of China spanning from 23°26′N to 40°0′N (Fig. 1), which included eight provinces and municipalities: Liaoning (LN), Hebei (HB), Tianjin (TJ), Shandong (SD), Jiangsu (JS), Shanghai (SH), Zhejiang (ZJ), and Fujian (FJ). A total of 21 National Nature Reserves (NNRs) are located within the study area (Wang et al., 2021b) and some of them are rampantly invaded by *Spartina*, including the Yellow River Delta NNR (YRDNNR) in Shandong, Yancheng NNR (YNNR) in Jiangsu, Dafeng Milu NNR (DMNNR) in Jiangsu, Chongming Dongtan NNR (CDNNR) in Shanghai, Jiuduansha Wetland NNR (JWNNR) in Shanghai, Minjiang River Estuary NNR (MRENNR) in Fujian, and Zhangjiangkou Mangrove NNR (ZMNNR) in Fujian.

2.2. Data

2.2.1. Landsat data

The Google Earth Engine (GEE), a cloud computing platform, hosts several Landsat data products (Gorelick et al., 2017). We used the United States Geological Survey (USGS) Landsat 5/7/8 surface reflectance (SR) data during the period between 1985 (1985/1/1) and 2020 (2021/1/1), and processed them in the GEE platform. Landsat provides multispectral images with a 30-m spatial resolution and a 16-day revisit period. The atmospheric correction for Landsat SR data was conducted through the Landsat Ecosystem Disturbance Adaptive Processing System (LEDAPS) algorithm and Landsat Surface Reflectance Code (LaSRC) algorithm (Masek et al., 2006; Vermote et al., 2016). Bad-quality observations, including clouds, cloud shadows, and cirrus, were identified and removed according to the pixel quality attributes in the data files (Zhu and Woodcock, 2012). The study area covered 30 paths/rows (tiles) of the Landsat Worldwide Reference System (WRS-2) (Fig. 1).

We used the good-quality time series Landsat SR data to calculate four vegetation indices (VIs) (see Eqs. (1)–(4)): Normalized Difference Vegetation Index (NDVI), Enhanced Vegetation Index (EVI), Land Surface Water Index (LSWI), and modified Normalized Difference Water Index (mNDWI) (Huete et al., 2002; Tucker, 1979; Xiao et al., 2005; Xu, 2006). These four VIs have been widely used for coastal wetland classification (Chen et al., 2017; Wang et al., 2018; Wang et al., 2020; Zhang et al., 2020b). Both NDVI and EVI are good indicators of vegetation greenness and have been widely used in vegetation canopy and phenology studies (Zhang et al., 2003). LSWI is related to canopy and soil moisture, and a change from positive LSWI values to negative LSWI values represents a state change from green leaves to senescent leaves (Xiao et al., 2009). mNDWI is sensitive to surface water and is one of the most widely used index for identifying surface water bodies (Zhou et al., 2017).

$$\mathrm{NDVI} = \frac{\rho_{NIR} - \rho_{Red}}{\rho_{NIR} + \rho_{Red}} \quad (1)$$

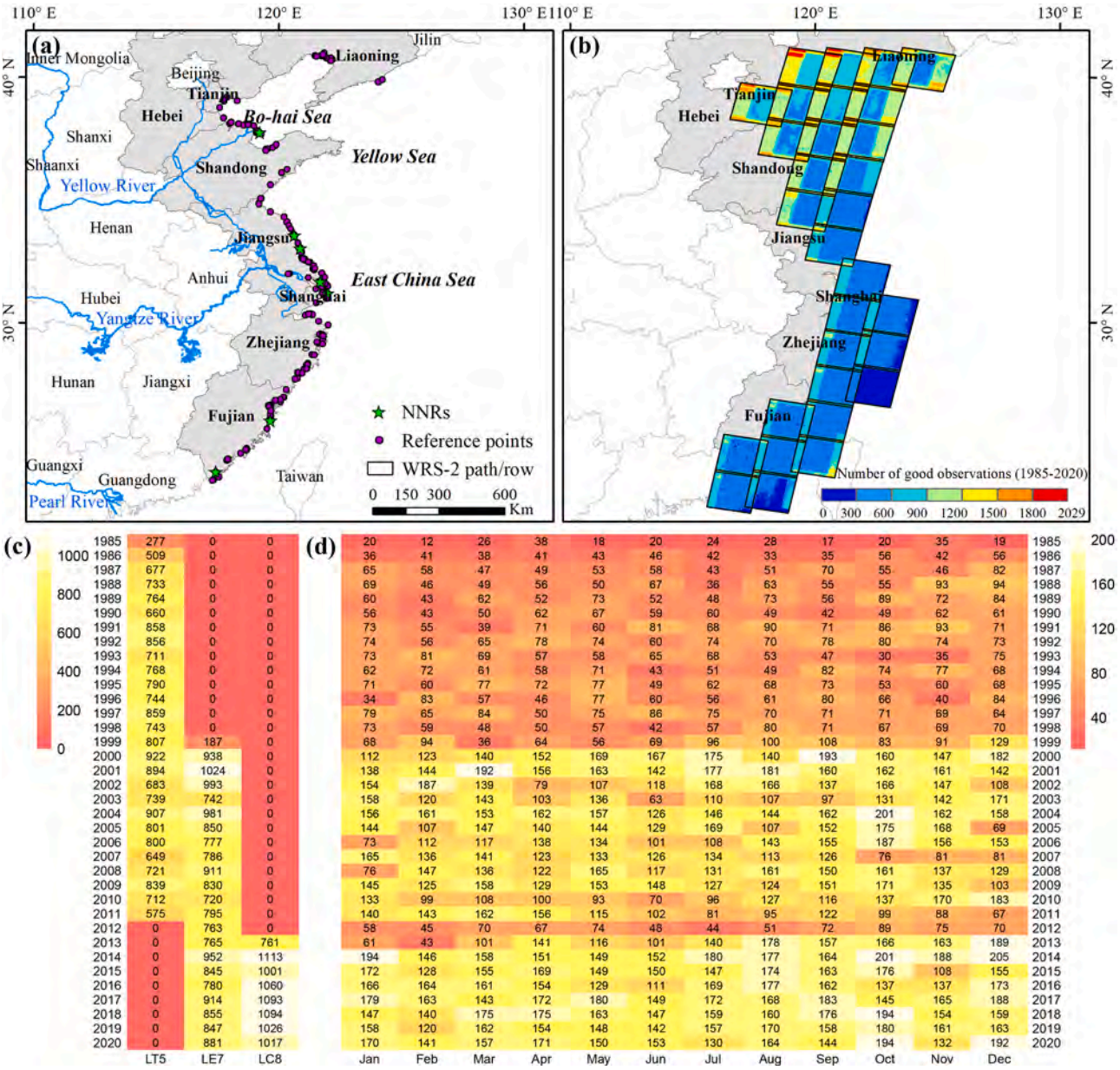

Fig. 1. The spatial distributions of the study area (a) and good-quality Landsat observations at individual pixels in the temperate and subtropical coastal zones of China during 1985–2020 (b), and the annual distributions of Landsat images from 1985 to 2020 divided by sensor (c) and month (d).

$$\mathrm{EVI} = 2.5 \times \frac{\rho_{NIR} - \rho_{Red}}{\rho_{NIR} + 6 \times \rho_{Red} - 7.5 \times \rho_{Blue} + 1} \tag{2}$$

$$\mathrm{LSWI} = \frac{\rho_{NIR} - \rho_{SWIR}}{\rho_{NIR} + \rho_{SWIR}} \tag{3}$$

$$\mathrm{mNDWI} = \frac{\rho_{Green} - \rho_{SWIR}}{\rho_{Green} + \rho_{SWIR}} \tag{4}$$

where ρ_{Blue}, ρ_{Green}, ρ_{Red}, ρ_{NIR}, ρ_{SWIR} are the surface reflectance values of the blue, green, red, near-infrared, and shortwave-infrared (1550–1750 nm for Thematic Mapper/Enhanced Thematic Mapper Plus (TM/ETM+) imagery and 1570–1650 nm for Operational Land Imager (OLI) imagery) bands in Landsat images, respectively.

2.2.2. Ground reference data

The ground reference data of *Spartina* saltmarshes and other native saltmarshes (hereafter, non-*Spartina*) came from two sources: (1) georeferenced photos taken during field surveys and (2) geographic coordinates published in previous studies or by data centers. First, a large-scale field survey was conducted in August and September in 2015, and another field survey was conducted in July and September in 2020. During the field survey, we took geo-referenced photos using digital single-lens reflex (DSLR) camera and collected optical images using DJI Phantom 4 Pro unmanned aerial vehicle (UAV). Based on the field photos, UAV data, and very high spatial resolution (VHSR) images from Google Earth, we constructed the ground reference datasets circa 2015. Second, we collected geographic coordinates of *Spartina* saltmarshes published in previous studies (Liu et al., 2018; Zhang et al., 2020a) and those of non-*Spartina* saltmarshes provided by the National Earth System Science Data Center, National Science & Technology Infrastructure of China (http://www.geodata.cn). We organized these data into a database and used them as references to supplement the ground reference datasets. As the published geo-location information (latitude and longitude) was mostly recorded from field surveys during 2013–2017, we visually inspected individual data points and removed those inappropriate points. Finally, a total of 174 *Spartina* saltmarsh

ground reference points and 163 non-*Spartina* saltmarsh ground reference points were obtained.

How to select and partition sample data for training and validation is important for reducing sampling bias and ensuring representativeness of the results. To reduce the bias that might arise from spatial autocorrelation, we first divided the whole study area into 50 nonoverlapping grids (1° latitude by 1° longitude). We then randomly selected 40% of these grids (~13% in each subregion referring to section 2.3.1), and in these grids randomly selected 40% of the *Spartina* and non-*Spartina* saltmarsh ground reference points as training points. Note that for the training datasets, we used only the data points collected from field surveys, and ensured that each point covered patches larger than 60 m × 60 m. Each training point was then used to delineate the training regions of interest (ROIs) as circle buffers of the points (15-m radius). Finally, 41 *Spartina* ROIs containing a total of 453 pixels and 29 non-*Spartina* ROIs containing a total of 319 pixels were obtained, which were constructed as the training dataset (Tabs. S1–S2). As we used knowledge-based algorithm to identify and map land cover types, we also considered the training dataset as the learning dataset. For the pixels in the learning dataset (or training dataset), we analyze time series image data to learn and gain knowledge of land cover types in the pixels.

2.3. Mapping algorithm

2.3.1. Subregions of the study area

In our previous study conducted on Chongming island, Shanghai, two phenological features of *Spartina* saltmarshes were identified, and these features were used to differentiate *Spartina* saltmarshes from other types of saltmarshes and to develop a pixel- and phenology-based *Spartina* saltmarsh mapping algorithm (Zhang et al., 2020b). It should be noted that *Spartina* saltmarsh and other saltmarshes vary latitudinally in phenological characteristics (Zhang et al., 2022), especially under the background of high dynamic and heterogeneous coastal environments. Therefore, the classification strategy should also be adapted from region to region. The reasonable regional divisions can improve the efficiency of mapping algorithm and the accuracy of resulting maps (Hu et al., 2021).

The phenological traits of *Spartina* and the local tidal dynamics were considered in this study when delineating the study area. An early work (Zhang et al., 2022) investigated the latitudinal changes in *Spartina* saltmarsh phenology and found a significantly linear latitudinal trend in the start of growing season (SOS). We first divided the study area into two subregions based on the SOS ranges: (1) high-latitude (HL) region (35°N − 40°N, DOY 150–180), corresponding to the temperate zone and (2) middle-latitude region (23.5°N − 35°N, DOY 120–150), corresponding to the subtropical zone. This division could facilitate the definition of regional spring temporal windows. In addition, according to the mean tidal range (MTR) calculated using the vertical height differences between high and low water levels published by the National Marine Data Center (http://mds.nmdis.org.cn/), we further partitioned the middle-latitude region into the middle-latitude-north region (MLN; 30°N − 35°N, MTR < 5 m) and the middle-latitude-south region (MLS; 23.5°N − 30°N, MTR > 5 m). Therefore, three subregions (i.e., the HL, MLN, and MLS regions) were defined (Table 1).

2.3.2. Phenology-based Spartina saltmarsh mapping

The seasonal dynamics of three vegetation indices (NDVI, EVI, and LSWI) calculated at selected *Spartina* and non-*Spartina* sites (one species by one site) in three subregions were compared (Fig. 2). It was clear that spring and winter were the good seasons for discriminating *Spartina* saltmarshes from non-*Spartina* saltmarshes. In early spring, other saltmarshes start to green up, having positive LSWI values (>0), while *Spartina* saltmarshes do not start to green up, having negative LSWI values (<0). The frequency histograms derived from training ROIs (Fig. 3) indicated that the mean LSWI values from May to June

Table 1
Characteristics of the three subregions in the temperate and subtropical coastal zones of China.

Subregion	Latitude range	SOS range (DOY)	Mean tidal range (m)	Provinces/ municipalities
HL region	35°N-40°N	150–180	<5	Liaoning, Hebei, Tianjin, Shandong
MLN region	30°N-35°N	120–150	<5	Jiangsu, Shanghai
MLS region	23.5°N-30°N	120–150	>5	Zhejiang, Fujian

Note: The abbreviations HL, MLN, and MLS denote the high-latitude, middle-latitude-north, and middle-latitude-south regions, respectively.

($LSWI_{mean(May\text{-}June)}$) and from April to May ($LSWI_{mean(April\text{-}May)}$) could discriminate *Spartina* saltmarshes from non-*Spartina* saltmarshes in high-latitude and middle-latitude regions, respectively; and the corresponding $LSWI_{mean}$ thresholds were determined to be 0 and 0.4, respectively, by assessing the proportions of *Spartina* saltmarsh pixels. In winter, *Spartina* saltmarshes have high NDVI (>0.2), EVI (>0.1), and LSWI (>0) values, which can be regarded as green vegetation signals (Eq. (5)). The period from December to January was found to be a good time to discriminate *Spartina* saltmarshes from non-*Spartina* saltmarshes in both high-latitude and middle-latitude regions. We calculated the green vegetation frequencies (VFs) for individual pixels using Eq. (6), and the resulting frequency histogram showed that $VF_{(Dec\text{-}Jan)}$ values greater than 0 could differentiate *Spartina* saltmarshes from non-*Spartina* saltmarshes in this period (Fig. 3). In summary, the decision rules established for identifying *Spartina* saltmarshes in the HL, MLN, and MLS regions are shown in Eqs. (7) –(9).

$$Vegetation = NDVI \geq 0.2 \cap EVI \geq 0.1 \cap LSWI > 0 \quad (5)$$

$$VF = \frac{N_{Vegetation}}{N_{Good}} \quad (6)$$

$$Spartina\ saltmarshes_{HL\ region} = LSWI_{mean(May-Jun)} \leq 0 \cap VF_{(Dec-Jan)} > 0 \quad (7)$$

$$Spartina\ saltmarshes_{MLN\ region} = LSWI_{mean(Apr-May)} \leq 0 \cap VF_{(Dec-Jan)} > 0 \quad (8)$$

$$Spartina\ saltmarshes_{MLS\ region} = LSWI_{mean(Apr-May)} \leq 0.4 \cap VF_{(Dec-Jan)} > 0 \quad (9)$$

where *VF* is the vegetation frequency scaled between 0 and 1 in a year, $N_{Vegetation}$ corresponds to the number of observations determined as green vegetation in a year, and N_{Good} corresponds to the number of good-quality observations in a year.

2.3.3. Regional implementation of the mapping algorithm

The delineation of coastal zones and identification of coastal vegetation areas can help reduce commission errors when generating *Spartina* saltmarsh maps. We visually interpreted VHSR images on Google Earth at a scale of 1:24,000 to delineate the coastline each year (Wang et al., 2020). A 20-km seaward buffer was created as potential coastal zones. Next, we generated coastal vegetation maps using the decision tree classification scheme developed in previous studies (Wang et al., 2018; Wang et al., 2020). For each pixel, all good-quality observations within a year were determined as green vegetation or non-green vegetation using Eq. (5) and were similarly determined as water or non-water using Eq. (10). The vegetation frequency (VF) and water frequency (WF) of each pixel were then calculated using Eqs. (6) and (11). We used a VF threshold of 0.15 (VF ≥ 0.15) and a WF threshold of 0.95 (WF ≤ 0.95) to delineate coastal vegetation. Furthermore, we produced annual mangrove maps, following the algorithms proposed by Chen et al. (2017) and refined by Wang et al. (2021b), as mask layers to delineate

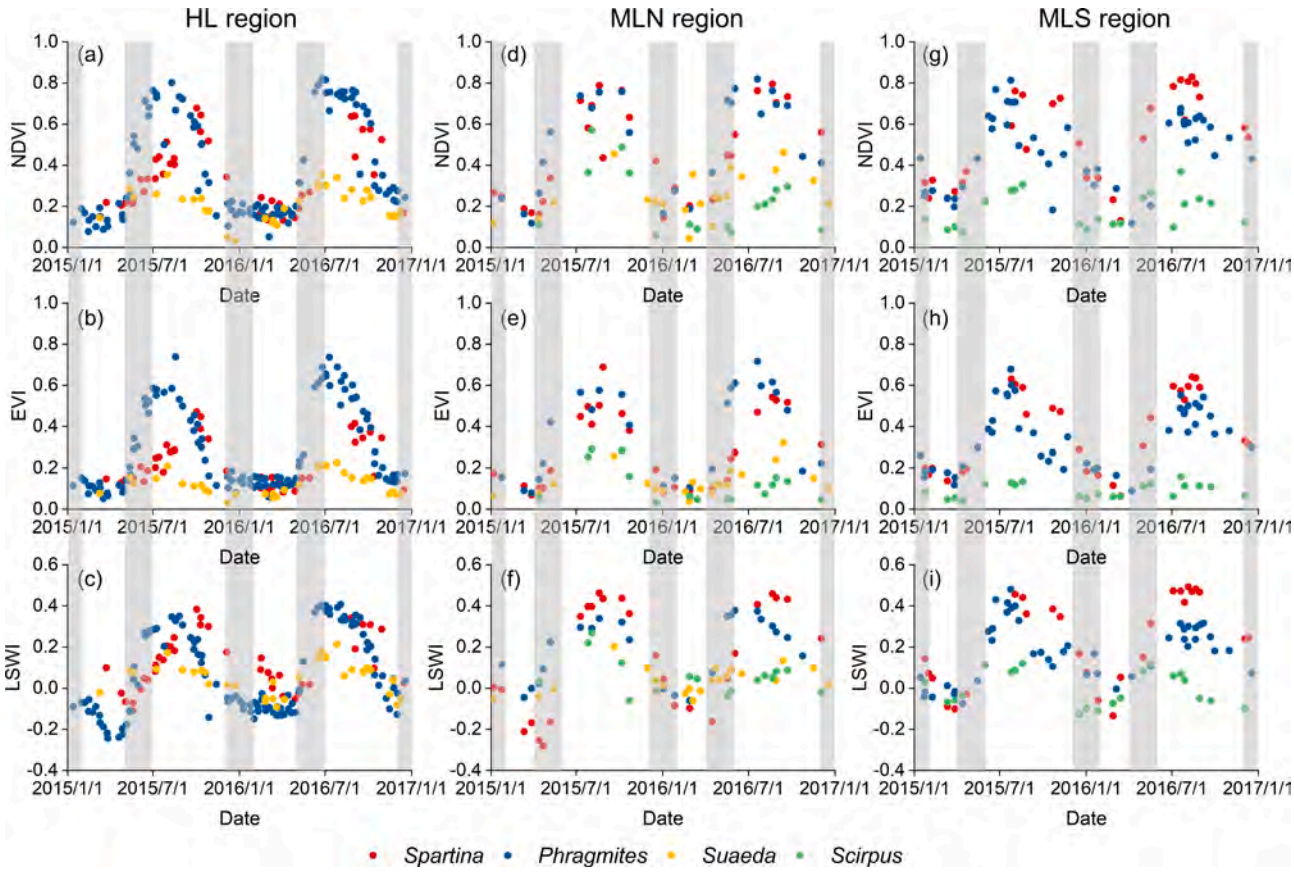

Fig. 2. Seasonal dynamics of three vegetation indices in three subregions during 2015–2016. The dominant saltmarsh species in each region are presented.

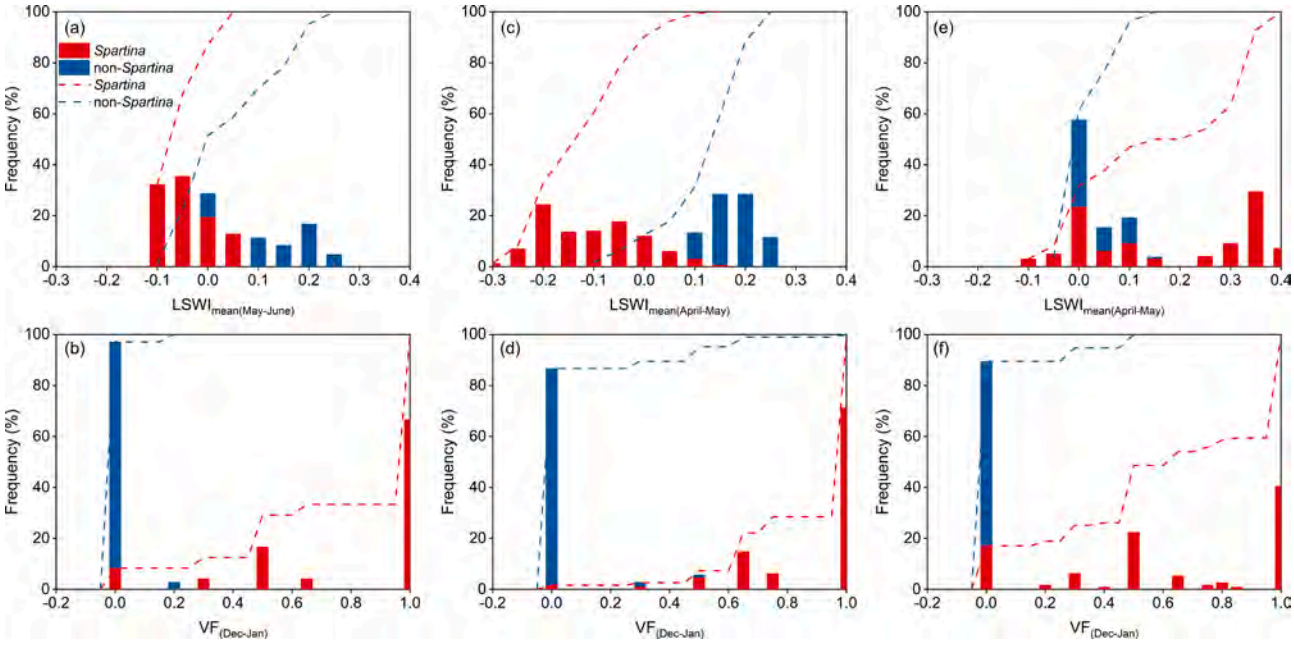

Fig. 3. Frequency histograms of *Spartina* and non-*Spartina* saltmarshes among $LSWI_{mean}$ and VF values in the HL region (a-b), MLN region (c-d), and MLS region (e-f) in 2015. The dashed lines indicate the corresponding cumulative frequencies.

saltmarshes. The decision rules of DEM $\leq$ 6 m and slope $\leq 6^{\circ}$ were used as supplementary criteria to limit the potential distributions *Spartina* saltmarshes (Fig. S1). The detailed workflow is shown in Fig. 4.

$$Water = (mNDWI > EVI \ or \ mNDWI > NDVI) \cap EVI < 0.1 \quad (10)$$

$$WF = \frac{N_{Water}}{N_{Good}} \quad (11)$$

Because of the frequent presence of clouds in coastal regions, many pixels often had small number of good-quality observations within a

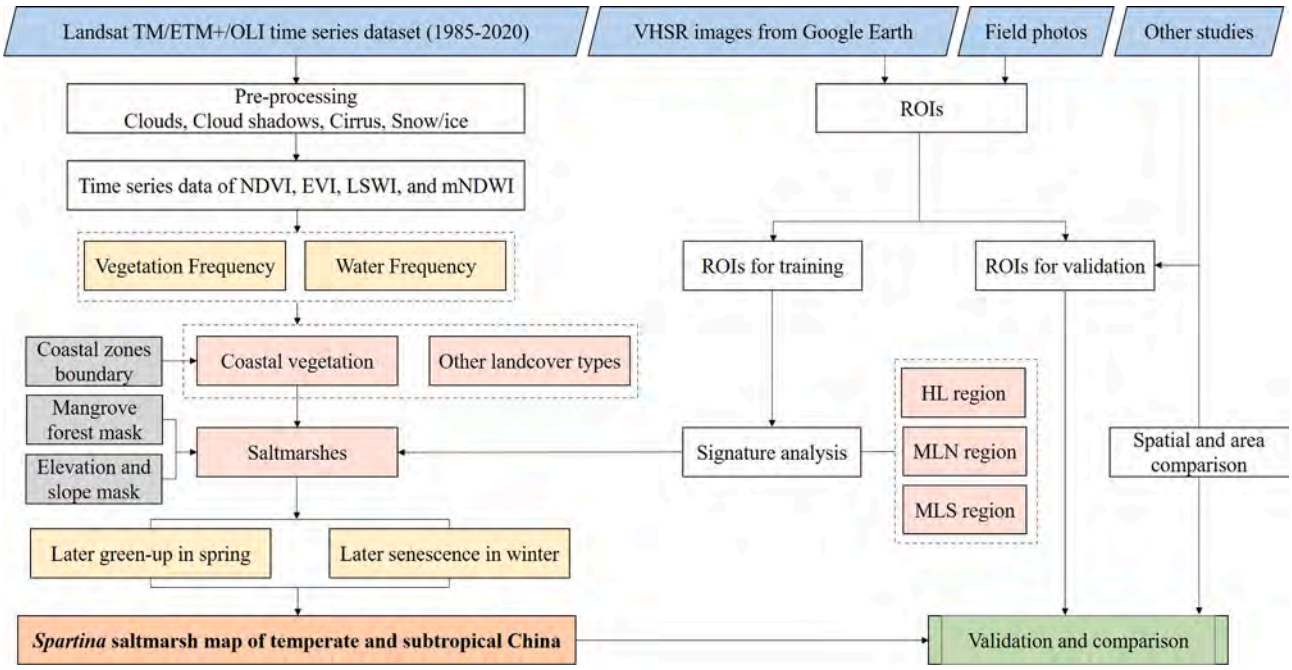

Fig. 4. Workflow for mapping *Spartina* saltmarshes in the temperate and subtropical coastal zones of China.

year and thus, *Spartina* saltmarsh maps resulting from analyses of images within a year might have been subject to large underestimation. To address this data issue, we also generated *Spartina* saltmarsh maps using satellite images acquired within 3-year (y-1, y, and y+1) and 5-year (y-2, y-1, y, y+1, and y+2) windows. Specifically, we combined 3-year or 5-year satellite data to generate 1-year data, organized by day of year (DOY), and used these data to generate one *Spartina* saltmarsh map. For example, we produced the map of *Spartina* saltmarshes in 2018 within 3-year window by using satellite images from 2017 (2017/1/1) to 2019 (2019/12/31). We ended up with three sets of annual *Spartina* saltmarsh maps using 1-year satellite images (1-yr maps), 3-year satellite images (3-yr maps), and 5-year satellite images (5-yr maps).

2.4. Accuracy assessment of Spartina saltmarsh maps

Assessing the accuracy of *Spartina* saltmarsh maps was conducted through two approaches: (1) using reference data collected during in-situ surveys (RD_{ground}) and (2) using reference data obtained from visual interpretations of Google Earth VHSR images (RD_{image}) over pixels selected by the stratified random sampling method to assess the classified maps. With respect to the first validation approach, we overlaid the remaining 133 *Spartina* saltmarsh points and 134 non-*Spartina* saltmarsh points from the ground reference datasets on the classified map to check whether each point belonged to the corresponding category. Second, we generated random points in each stratum on the classified map by using a stratified random sample function in the GEE platform. As an early study (Hu et al., 2021) has reported that *Spartina* saltmarshes (48.3%) and non-*Spartina* saltmarshes (51.7%) existed in comparatively similarly sized areas along coastal China in 2019, the same number of points were therefore generated for each stratum. Specifically, for each grid over temperate and subtropical coastal China, 10 points were randomly generated on the *Spartina* and non-*Spartina* saltmarsh maps. The points lacking clear land cover information due to unavailable Google Earth VHSR images were excluded. To ensure the same number of validation points obtained in each map (i.e., 1-yr, 3-yr, and 5-yr maps), we further randomly selected points among the generated points. In total, 356 *Spartina* points and 355 non-*Spartina* points in each map were used to construct the validation dataset (Tabs. S1–S2). Each point was interpreted visually on Google Earth to determine the land cover type in the image pixel. We calculated the confusion matrix to estimate the accuracy of the resulting maps.

2.5. Statistical analysis

2.5.1. Analysis of spatiotemporal dynamics of Spartina saltmarshes

At the pixel scale, there were three scenarios for one single pixel in a year: identified as *Spartina* saltmarshes (value as 1), identified as non-*Spartina* saltmarshes (value as 0), or not enough data to be classified (value as −1) (Fig. 5). Some pixels previously identified as *Spartina* saltmarshes might not recognize *Spartina* saltmarshes for one or two years due to missing satellite imagery data. Therefore, we used the annual *Spartina* saltmarsh maps generated from 5-year satellite data to delineate the changes in *Spartina* saltmarshes from 1990 to 2018.

We quantified the spatial variations of *Spartina* saltmarshes by calculating the differences in pixel values between the previous-year map and the current-year map. Three types of results were obtained by referencing Eq. (12): pixels labeled as having gain of *Spartina* saltmarshes (when value as 1), pixels labeled as having loss of *Spartina* saltmarshes (when value as −1), or pixels labeled as having no change (when value as 0). Both the frequency and period of gains and losses were extracted. In addition, we analyzed the first year in which a pixel was identified as *Spartina* saltmarshes during 1985–2020 by employing Eq. (13). The invasion history of *Spartina* was also analyzed by counting the number of times that a pixel was identified as *Spartina* saltmarshes using Eq. (14). To understand the latitudinal variations in *Spartina* saltmarshes, we aggregated the four indicators (gain frequency, loss frequency, first-time detection, and invasion history) at 0.1° latitudinal intervals.

$$Dynamics = \begin{cases} Gain_{(i)} & \left(Map_{(i)} - Map_{(i-1)} = 1\right) \\ Loss_{(i)} & \left(Map_{(i)} - Map_{(i-1)} = -1\right) \\ No\ change_{(i)} & \left(Map_{(i)} - Map_{(i-1)} = 0\right) \end{cases} \quad (12)$$

$$First_{(i)} = Map_{(i)} - Map_{(i-1)} - Map_{(i-2)} - \cdots - Map_{1990} \quad (13)$$

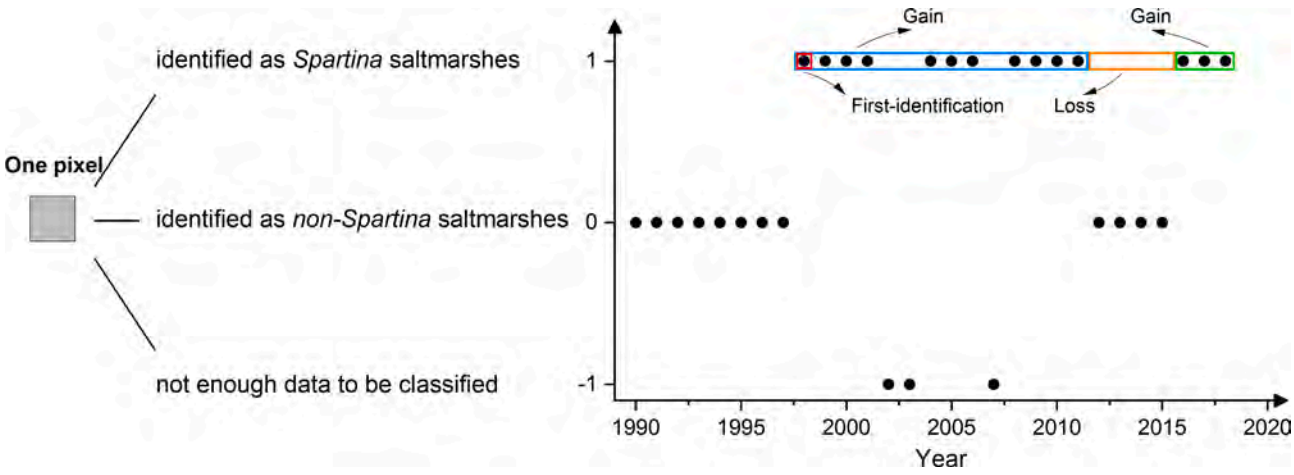

Fig. 5. Schematic diagram for identifying *Spartina* saltmarshes at the pixel level over a year.

$$Age = \sum_{i=1990}^{2018} Map_i \quad (14)$$

2.5.2. Analysis of driving factors of Spartina saltmarsh gains and losses

To analyze the driving factors of the observed *Spartina* saltmarsh gains and losses, we disaggregated and quantified the relative contributions of direct and indirect drivers. Direct drivers were defined as changes resulting from land conversion processes such as agriculture, aquaculture, urban and industrial development, lawns, riverways, coastal infrastructure, and other ecological engineering measures, most of which were related to human activities and could be observed from the Google Earth VHSR images (Fig. S2). Indirect drivers included the effects of natural coastal processes, climate change, vegetation dieback, erosion, and other remote drivers of land use changes, which were not directly observable on Google Earth VHSR images (Fig. S2). We mosaicked all the *Spartina* saltmarsh gain maps by choosing the earliest year in which *Spartina* was identified in overlapping areas and all the *Spartina* saltmarsh loss maps by choosing the latest year in which *Spartina* was identified in overlapping areas in ArcGIS software, as the earliest gain period could be connected to the artificial introduction history of *Spartina* and the latest loss period could rescue from lacking available images to interpret in the early years. On these two maps, we randomly sampled 5 gain or loss points in each grid of the 50 nonoverlapping grids described in section 2.2.2. We removed sample points at which the drivers were not clear when visually interpreted on Google Earth. Each sample point was labeled with a gain or loss year and the corresponding driver category.

3. Results

3.1. Accuracy assessment of annual Spartina saltmarsh maps

The accuracies of three *Spartina* saltmarsh maps in 2015 were assessed and compared, and the results indicated that all the maps had high accuracies (Table 2). The overall accuracies (OA) of 1-yr, 3-yr, and 5-yr *Spartina* saltmarsh maps were 83.0%, 88.2%, and 88.8%, respectively. The accuracy of 1-yr map was the lowest, with kappa coefficient of 0.66, and the accuracy of 5-yr map was the highest, with kappa coefficient of 0.77. The user's accuracy (UA) and producer's accuracy (PA) were improved by 4% – 8% when 3-year or 5-year satellite data were incorporated to generate the maps. The UAs were generally higher than the PAs in these three *Spartina* saltmarsh maps, indicating that the maps had higher omission errors than commission errors. We also compared the accuracy assessment results at the provincial scale and found that the OAs of all provinces were over 75% (Fig. S3). The UAs corresponding to low-latitude provinces were lower than those corresponding to other regions, indicating that misclassification was a major concern at relatively low latitudes. Moreover, relatively low PAs occurred in middle-latitude provinces, indicating that potential underestimation should be considered in these regions.

Table 2
Accuracy assessment results of *Spartina* saltmarsh and non-*Spartina* saltmarsh maps (1-yr map, 3-yr map, and 5-yr map) in 2015.

	1-yr map		3-yr map		5-yr map	
	Spartina	non-*Spartina*	*Spartina*	non-*Spartina*	*Spartina*	non-*Spartina*
UA	83.0%	83.1%	87.1%	89.3%	88.3%	89.2%
PA	80.4%	85.3%	88.1%	88.4%	88.3%	89.2%
OA	83.0%		88.2%		88.8%	
Kappa	0.66		0.76		0.77	

3.2. Interannual changes in Spartina saltmarsh areas from 1990 to 2018

Spartina spread over temperate and subtropical coastal China underwent continual expansion between 1990 and 2018. In 1990, there were 89.04 km^2 of *Spartina* saltmarshes, while the *Spartina* saltmarsh extent reached 517.89 km^2 in 2018, showing a significantly increasing trend (slope of 14.21 km^2 yr^{-1}). The *Spartina* saltmarsh areas started to increase in 1990 but stagnated or even slightly decreased during 2000–2005 and then substantially increased after 2010 (Fig. 6a). As such, the interannual trend of *Spartina* saltmarsh areas could be divided into three phases: a rapidly increasing phase between 1990 and 2000 (slope of 14.75 km^2 yr^{-1}), a moderately increasing phase between 2000 and 2010 (slope of 10.48 km^2 yr^{-1}), and a rapidly increasing phase between 2010 and 2018 (slope of 27.09 km^2 yr^{-1}) (Fig. 6d).

Spartina saltmarshes were distributed unevenly among provinces and mainly occurred in Zhejiang (201.11 km^2), Jiangsu (136.34 km^2), Fujian (94.24 km^2), and Shanghai (54.12 km^2), which together accounted for 93.8% of the total *Spartina* saltmarsh area over temperate and subtropical coastal China in 2018. In Zhejiang, Jiangsu, and Fujian, *Spartina* saltmarshes experienced a rapidly increasing phase from 1990 to 2000, a slightly increasing phase from 2000 to 2010 and another rapidly increasing phase from 2010 to 2018 (Fig. 6d). In contrast, *Spartina* saltmarshes in Shanghai started to significantly increase in 2005 and exhibited the largest increasing trend (slope of 4.91 km^2 yr^{-1}) during 2000–2010.

Spartina also rampantly invaded the seven national nature reserves (NNRs), and they could be divided into two groups. The first group included YRDNNR and ZMNNR and they had continually increasing trends after 2010. For example, the area of *Spartina* saltmarshes in

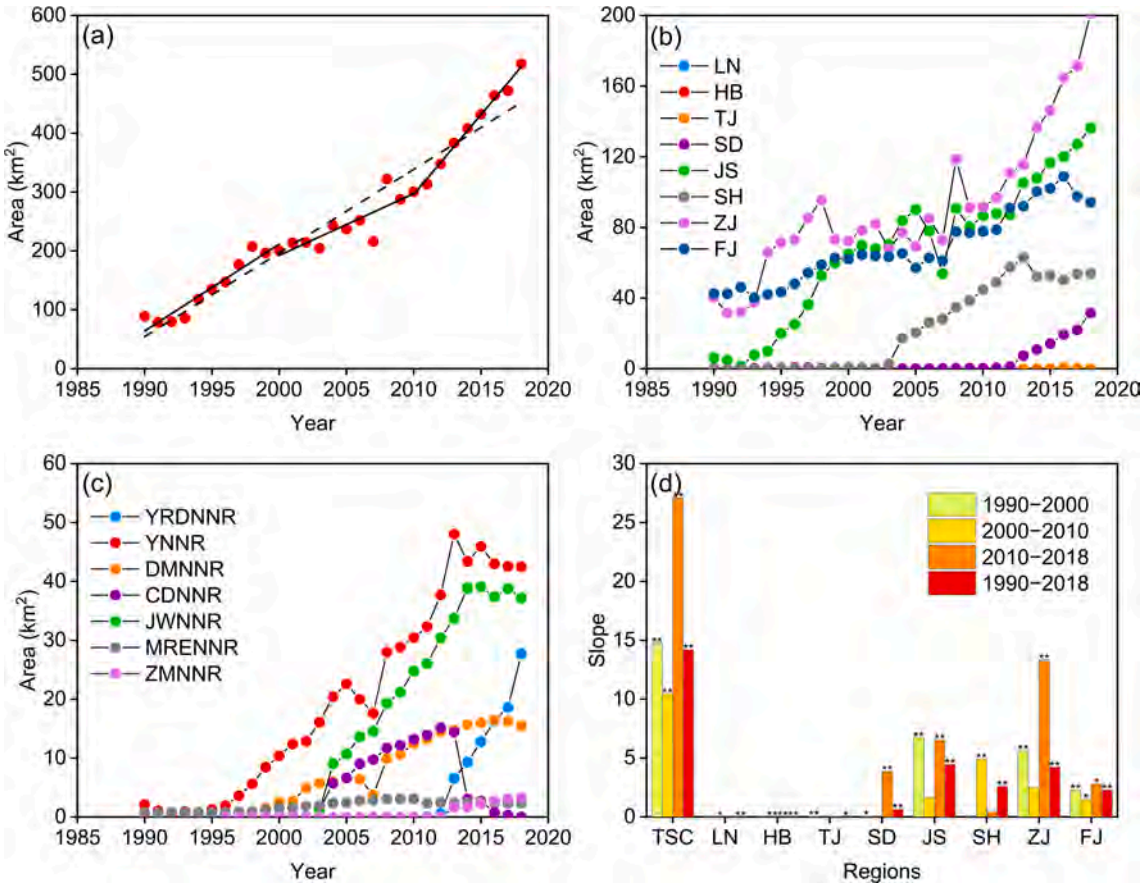

Fig. 6. The temporal dynamics of *Spartina* saltmarsh areas during 1990–2018 in the temperate and subtropical coastal zones of China (a), eight provinces/municipalities (b), and in seven national nature reserves (NNRs) (c). The black solid and dashed lines indicate *Spartina* saltmarsh trends in different periods. The linear trends and their significance levels in different periods in the temperate and subtropical coastal zones of China (TSC) and eight provinces/municipalities are also shown (d). * $p < 0.05$; ** $p < 0.01$.

YRDNNR increased from 0.57 km^2 in 2012 to 27.69 km^2 in 2018. The second group was composed of the other five NNRs and they experienced two distinct phases: a significantly increasing phase between 1990 and 2010 and a stagnant or significantly decreasing phase between 2010 and 2018. The area of *Spartina* saltmarshes in JWNNR had the largest increasing trend (slope of 2.91 km^2 yr^{-1}) from 1990 to 2010, but this

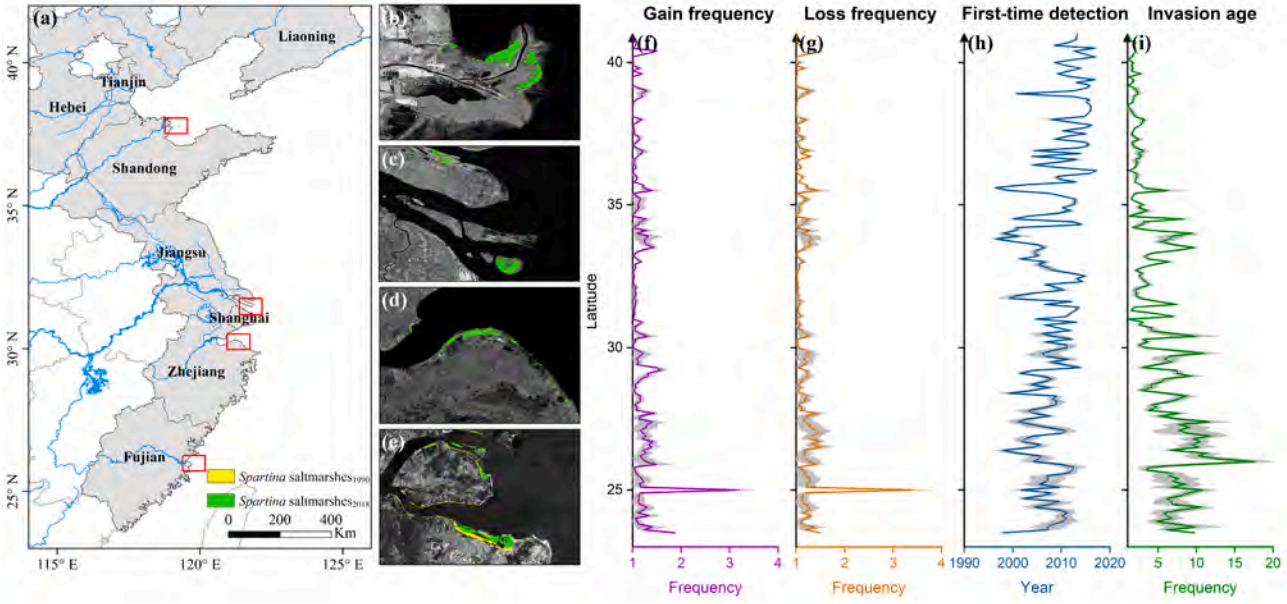

Fig. 7. The distribution of *Spartina* saltmarshes (a) and their latitudinal variations over temperate and subtropical coastal China during 1990–2018 (f-i). (b-e) Zoomed-in view of the four regions marked in (a). The shaded areas show the 95% confidence intervals.

area stagnated at approximately 38 km^2 after 2013. The most obvious decreasing trend occurred in CDNNR, where the *Spartina* saltmarsh extent decreased from 14.42 km^2 in 2013 to 3.08 km^2 in 2014 and then to 0.04 km^2 in 2018.

3.3. Spatial variations in Spartina saltmarshes during 1990–2018

The resulting maps showed that *Spartina* extensively invaded estuaries, bays, and deltas, such as Yellow River delta (Fig. 7b), Yangtze estuary (Fig. 7c), Hangzhou bay (Fig. 7d), and Minjiang estuary (Fig. 7e). Apart from the frequency spike observed in Fujian (~25°N), the gain and loss frequencies of *Spartina* saltmarshes were higher at low latitudes and lower at high latitudes (Fig. 7f-g). The years in which *Spartina* saltmarshes were first detected by Landsat images were earlier at low latitudes and later at high latitudes (Fig. 7h). *Spartina* saltmarshes occurred especially earlier in some estuaries, a finding connected to intentional introduction in the early years in these regions. Correspondingly, the invasion history of *Spartina* was longer at low latitudes and shorter at high latitudes (Fig. 7i). Moreover, the spatial variations in *Spartina* saltmarshes were quite different among seven NNRs (Fig. 8). In one case, *Spartina* rampantly replaced native plants and occupied more niches without human interventions. In another case, extensive *Spartina* saltmarshes were lost due to control and removal.

3.4. The effect of human activities on Spartina saltmarsh dynamics

Analyses of the random *Spartina* saltmarsh dynamic samples derived in the temperate and subtropical coastal zones of China suggested that 6% of gains and 75% of losses were attributed to human activities (as direct drivers) (Fig. 9). Among the eight provinces and municipalities, the *Spartina* saltmarsh dynamics was most driven by human activities in Shanghai, where 56% of gains and 86% of losses in *Spartina* saltmarshes were associated with intentional introductions in early years and human-induced land use conversions in recent years. Compared to *Spartina* saltmarsh gains, human activities played a more important role in *Spartina* saltmarsh losses. More than 60% of *Spartina* saltmarsh losses observed in Liaoning (97%), Hebei (86%), Tianjin (92%), Shandong (68%), Jiangsu (93%), Shanghai (86%), Zhejiang (100%), and Fujian (64%) were attributed to human activities. In contrast, most *Spartina* saltmarsh gains (94%) were caused by indirect drivers, highlighting that rapid natural spread was the prominent reason such extensive *Spartina* saltmarshes existed in the temperate and subtropical coastal zones of China.

4. Discussion

Many factors might affect the accuracy of the resulting *Spartina* saltmarsh maps from the analyses of satellite images, for example, saltmarsh definition, classification scheme, input imagery, training

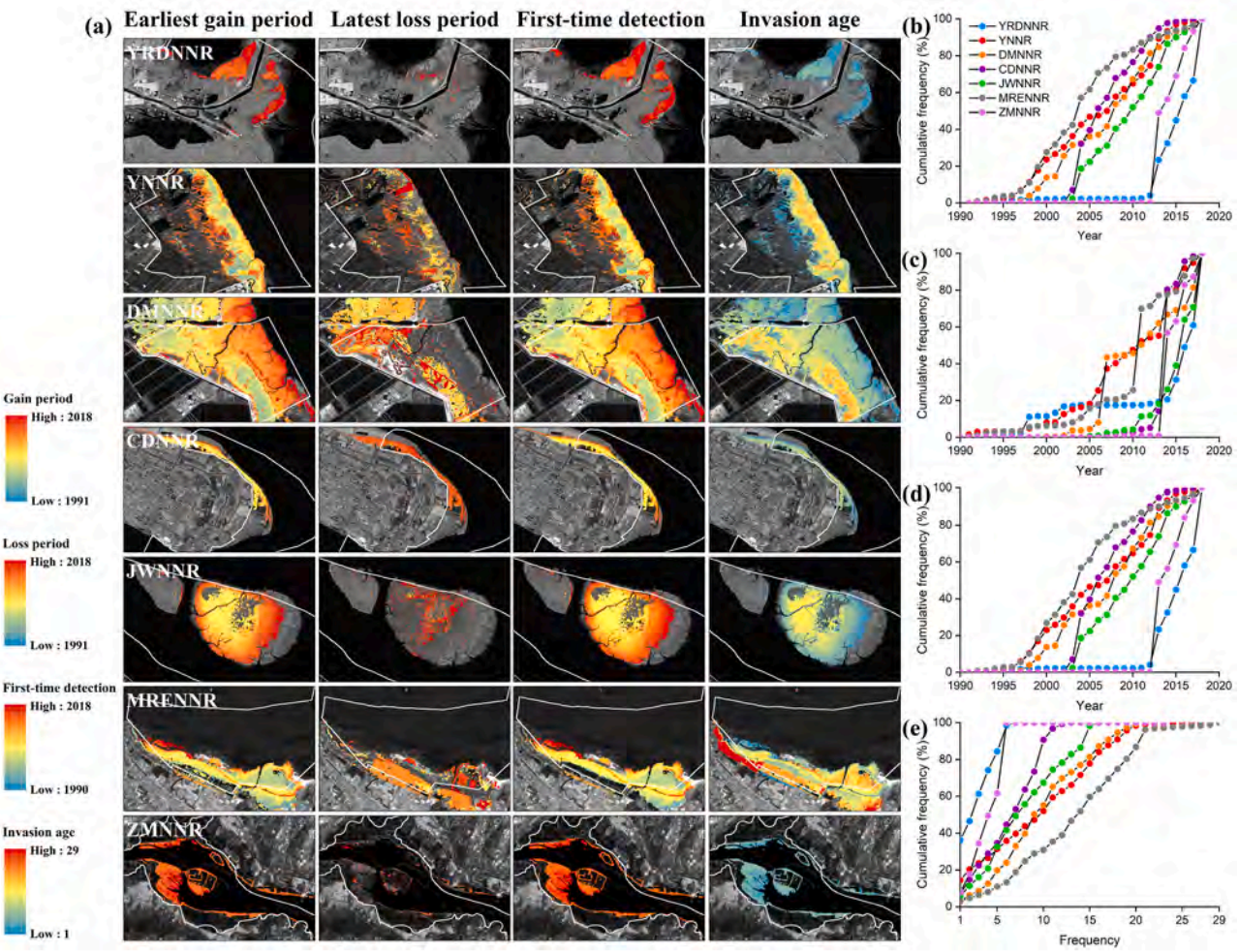

Fig. 8. The pixel-level dynamics of *Spartina* saltmarshes from 1990 to 2018 in seven NNRs. The earliest period of *Spartina* saltmarsh gains, the latest period of *Spartina* saltmarsh losses, the first year in which *Spartina* saltmarshes were identified, and the invasion ages of *Spartina* saltmarshes are shown with spatial details (a) and summarized by the cumulative pixel frequency (b-e). The white polygons indicate the boundaries of NNRs.

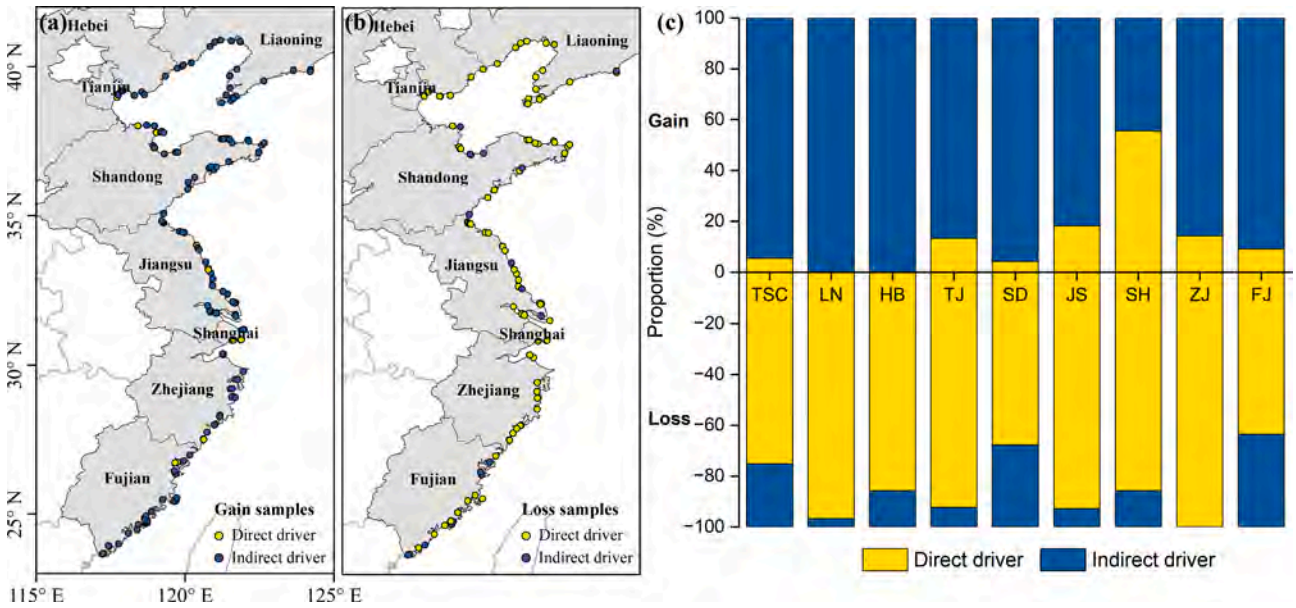

Fig. 9. The contributions of direct and indirect drivers to *Spartina* saltmarsh gains and losses during 1990–2018 in the temperate and subtropical coastal zones of China (TSC) and eight provinces/municipalities.

sample, and mapping algorithm. First, the applicability of the pixel- and phenology-based algorithm was subject to image quality in specific temporal windows during spring and winter. Based on our assessments, using satellite images from a single year was prone to omit some *Spartina* saltmarshes (Table 1). In addition, as Landsat images have 30-m spatial resolution, the algorithm did not identify those pixels with small proportions of *Spartina*, mostly at the early *Spartina* invasion stage. Second, the pixel- and phenology-based algorithm depends on our knowledge of phenology of various saltmarsh species, which may vary across the latitudes (Zhang et al., 2022). An early study reported that the difference in the start of growing season (SOS) between *Spartina* and *Phragmites* tended to decrease as the study sites moved to south (low latitudes) (Sun et al., 2021), making it difficult to apply SOS-based rules at relatively low latitudes. Third, the accurate location of the shoreline is a non-negligible factor affecting areal estimates, because we chose the 20-km seaward buffer as the potential *Spartina* distribution areas. Despite these concerns, the algorithm developed in this study could produce promising results that potentially enhance our understanding of the spatial and temporal dynamics of *Spartina* saltmarshes.

Our results showed that *Spartina* sustained a serious invasion trend over the period of 1985–2020 and linear increases in many coastal regions (Fig. 6). To conserve the native ecosystems, many nature reserves have been established and several prevention measures have been taken in coastal China (An et al., 2007; Yuan et al., 2011). For example, a large-scale ecological restoration project was carried out in CDNNR, Shanghai in 2013 to eradicate invasive *Spartina* within an area of 24.19 km^2 and investment of $186 million (Zhang et al., 2020b). However, the rampant expansion of *Spartina* has not been effectively reversed. The habitats for native saltmarshes over nature reserves have been largely invaded by *Spartina* (Fig. 8), including a world heritage site of the Migratory Bird Sanctuaries along the coast of Yellow Sea-Bohai Gulf of China. A recent study found that plant invasions in the protected areas were even more extensive and faster than those outside the protected areas (Ren et al., 2021b). Even for those regions that have undergone control programs, the subsequent *Spartina* reinvasion is frequent, making the restoration of native saltmarshes difficult (Zhang et al., 2020b; Zhao et al., 2020).

Considering the proximity of saltmarshes to human-related activities, the spatiotemporal dynamics of *Spartina* saltmarshes are inevitably influenced by human activities. On the one hand, the intentional introductions of *Spartina* have been deemed the most important factor for its invasion success (Meng et al., 2020). The *Spartina* saltmarsh gains observed in many coastal regions are inseparable from the planting of *Spartina* at the early stages, followed by the spread of seeds by the tide. On the other hand, the coastal reclamation is known to be a prominent anthropogenic factor affecting the distribution of saltmarshes in China (Chen et al., 2022). Specifically, reclamations can accelerate *Spartina*'s seaward expansion by changing the sedimentary environment of mudflats in front of dikes and causing extensive fine-particle sedimentation, which provides a suitable environment for *Spartina* colonization and growth (Zhu et al., 2022). However, land cover changes induced by human activities caused *Spartina* saltmarsh losses more frequently than gains. For example, although *Spartina* has a high expansion capability, the coastal reclamation pace being faster than the *Spartina* growth rate would lead to *Spartina* saltmarsh losses, not to mention destroying the habitats of *Spartina* and reducing *Spartina* seed yields. Our sample-based driving factor analysis showed that compared to ~5% of *Spartina* saltmarsh gains, more than 70% of *Spartina* saltmarsh losses could be attributed to human activities. Interestingly, the continual natural spread and expansion of *Spartina* offset the *Spartina* saltmarsh losses caused by human activities and resulted in net *Spartina* saltmarsh increases in the temperate and subtropical coastal zones of China over the past decades.

In an early literature review paper (Vaz et al., 2018), the authors have summarized that remote sensing technology has been applied for identification of invasive species since the late 1970s, for prediction of potential distributions of invasive species later, and recently for assessments of impacts of invasive species on ecosystems. Research on invasion dynamics of individual invasive species and their impacts on local environments can provide more information to manage *Spartina* invasions in an efficient and integrated manner. It has been reported that approximately 803 km^2 of mudflats and 29 km^2 of saltmarshes have been converted to *Spartina* saltmarshes in coastal China during 1990–2015 (Mao et al., 2019), which directly changes the composition and distribution of coastal wetlands. As a valuable resource for people to combat global warming, conserving the integrity of ecosystem structure and functions of coastal wetlands is critical for achieving the carbon neutrality in China by 2060. In summary, the identification of invasive *Spartina* is the first and crucial step; however, how to adapt, mitigate, and reduce its extensive invasion is still a topic that needs to be explored.

5. Conclusion

Overwhelming *Spartina alterniflora* invasions have seriously threatened the structure and functions of coastal ecosystems in China, which is widely recognized as a major ecological and environmental issue. This study improved the pixel- and phenology-based *Spartina* saltmarsh mapping algorithm and provided a new dataset of *Spartina* saltmarshes in the temperate and subtropical coastal zones of China over the past three decades. The resulting *Spartina* saltmarsh maps have reasonably high accuracy. Relatively higher omission errors than commission errors indicates that more high-quality time series observations are needed, which can be achieved by incorporating Landsat 9 and Sentinel-1 images. Although considerable efforts have been made to control *Spartina* invasions and various human interventions have reduced *Spartina* saltmarshes in some parts of the coastal China, the resulting maps reveal that *Spartina* saltmarshes have been continually expanding at high rates in many parts of coastal China. Our work also reveals the spatial variations in *Spartina* invasion over the latitudinal gradient from the temperate zone to the subtropical zone. The annual *Spartina* saltmarsh maps during 1985–2020 can be used to support future work that aims to select hot-spots for *Spartina* control, predict potential regions for *Spartina* expansion, and assess the impacts of *Spartina* invasion and expansion on coastal wetland biodiversity and ecosystem services. To achieve ecological security and the sustainability of coastal wetlands in China remains to be a grand challenge for the years to come, and remote sensing of coastal wetlands can play an increasingly important role for decision makers, stakeholders and the public.

Author contributions

X.Z., X.X., and B.L. designed the study; X.Z. and X.X. conducted the analysis; X.W. contributed to the algorithm development; X.X. and S.Q. contributed to the result interpretation and discussion; L.P., J.M., R.J., and J.W. provided the field survey data; and X.Z., X.X., and B.L. led the writing of the manuscript.

Correspondence and requests for materials should be addressed to Xiangming Xiao or Bo Li.

Declaration of Competing Interest

The authors declare that they have no known competing financial interests or personal relationships that could have appeared to influence the work reported in this paper.

Data availability

Data will be made available on request.

Acknowledgements

The study was supported by National Key Research and Development Program of China (2022YFC2601100), the National Natural Science Foundation of China (32030067, 32171661, 41630528, and 42201341), the Special Project on National Science and Technology Basic Resources Investigation of China (2021FY100704), the U.S. National Science Foundation (1911955), and the China Postdoctoral Science Foundation (2021M700835 and 2021TQ0072). We sincerely appreciate the data support from National Earth System Science Data Center (http://www.geodata.cn) and National Marine Data Center (http://mds.nmdis.org.cn/), National Science & Technology Infrastructure of China.

Appendix A. Supplementary material

Supplementary data to this article can be found online at https://doi.org/10.1016/j.jag.2023.103192.

References

An, S., Gu, B., Zhou, C., Wang, Z., Deng, Z., Zhi, Y., Li, H., Chen, L., Yu, D., Liu, Y., 2007. Spartina Invasion in China: implications for Invasive Species Management and Future Research. Weed Res. 47, 183–191.

Chen, B., Xiao, X., Li, X., Pan, L., Doughty, R., Ma, J., Dong, J., Qin, Y., Zhao, B., Wu, Z., Sun, R., Lan, G., Xie, G., Clinton, N., Giri, C., 2017. A mangrove forest map of China in 2015: Analysis of time series Landsat 7/8 and Sentinel-1A imagery in Google Earth Engine cloud computing platform. ISPRS J. Photogramm. Remote Sens. 131, 104–120.

Chen, G., Jin, R., Ye, Z., Li, Q., Gu, J., Luo, M., Luo, Y., Christakos, G., Morris, J., He, J., Li, D., Wang, H., Song, L., Wang, Q., Wu, J., 2022. Spatiotemporal mapping of salt marshes in the intertidal zone of China during 1985–2019. J. Remote Sens. 2022, 1–15.

Chen, M., Ke, Y., Bai, J., Li, P., Lyu, M., Gong, Z., Zhou, D., 2020. Monitoring early stage invasion of exotic Spartina alterniflora using deep-learning super-resolution techniques based on multisource high-resolution satellite imagery: a case study in the Yellow River Delta, China. Int. J. Appl. Earth Obs. 92, 102180.

Chung, C.H., 2006. Forty years of ecological engineering with Spartina plantations in China. Ecol. Eng. 27, 49–57.

Civille, J.C., Sayce, K., Smith, S.D., Strong, D.R., 2005. Reconstructing a century of Spartina alterniflora invasion with historical records and contemporary remote sensing. Ecosci. 12, 330–338.

Dawson, W., Moser, D., van Kleunen, M., Kreft, H., Pergl, J., Pysek, P., Weigelt, P., Winter, M., Lenzner, B., Blackburn, T.M., Dyer, E.E., Cassey, P., Scrivens, S.L., Economo, E.P., Guenard, B., Capinha, C., Seebens, H., Garcia-Diaz, P., Nentwig, W., Garcia-Berthou, E., Casal, C., Mandrak, N.E., Fuller, P., Meyer, C., Essl, F., 2017. Global hotspots and correlates of alien species richness across taxonomic groups. Nat. Ecol. Evol. 1, 0186.

Gorelick, N., Hancher, M., Dixon, M., Ilyushchenko, S., Thau, D., Moore, R., 2017. Google Earth Engine: Planetary-scale geospatial analysis for everyone. Remote Sens. Environ. 202, 18–27.

Gu, J., Jin, R., Chen, G., Ye, Z., Li, Q., Wang, H., Li, D., Christakos, G., Agusti, S., Duarte, C.M., Luo, Y., Wu, J., 2021. Areal extent, species composition, and spatial distribution of coastal saltmarshes in China. IEEE J Sel. Top. Appl. Earth Observ. Remote Sens. 14, 7085–7094.

Hu, Y., Tian, B., Yuan, L., Li, X., Huang, Y., Shi, R., Jiang, X., Wang, l., Sun, C., 2021. Mapping coastal salt marshes in China using time series of Sentinel-1 SAR. ISPRS J. Photogramm. Remote Sens. 173, 122-134.

Huete, A., Didan, K., Miura, T., Rodriguez, E.P., Gao, X., Ferreira, L.G., 2002. Overview of the radiometric and biophysical performance of the MODIS vegetation indices. Remote Sens. Environ. 83, 195–213.

Kirwan, M.L., Guntenspergen, G.R., Morris, J.T., 2009. Latitudinal trends in Spartina alterniflora productivity and the response of coastal marshes to global change. Glob. Chang. Biol. 15, 1982–1989.

Kirwan, M.L., Megonigal, J.P., 2013. Tidal wetland stability in the face of human impacts and sea-level rise. Nature 504, 53–60.

Li, B., Liao, C., Zhang, X., Chen, H., Wang, Q., Chen, Z., Gan, X., Wu, J., Zhao, B., Ma, Z., Cheng, X., Jiang, L., Chen, J., 2009. Spartina alterniflora invasions in the Yangtze River estuary, China: an overview of current status and ecosystem effects. Ecol. Eng. 35, 511–520.

Li, H., Mao, D., Wang, Z., Huang, X., Li, L., Jia, M., 2022. Invasion of Spartina alterniflora in the coastal zone of mainland China: control achievements from 2015 to 2020 towards the Sustainable Development Goals. J. Environ. Manage. 323, 116242.

Li, R., Yu, Q., Wang, Y., Wang, Z.B., Gao, S., Flemming, B., 2018. The relationship between inundation duration and Spartina alterniflora growth along the Jiangsu coast, China. Estuar. Coast. Shelf Sci. 213, 305–313.

Liu, M., Mao, D., Wang, Z., Li, L., Man, W., Jia, M., Ren, C., Zhang, Y., 2018. Rapid Invasion of Spartina alterniflora in the Coastal Zone of Mainland China: New Observations from Landsat OLI Images. Remote Sens. 10, 1933.

Mao, D., Liu, M., Wang, Z., Li, L., Man, W., Jia, M., Zhang, Y., 2019. Rapid invasion of spartina alterniflora in the coastal zone of Mainland China: spatiotemporal patterns and human prevention. Sensors 19, 2308.

Masek, J.G., Vermote, E.F., Saleous, N.E., Wolfe, R., Hall, F.G., Huemmrich, K.F., Gao, F., Kutler, J., Lim, T.K., 2006. A Landsat Surface Reflectance Dataset for North America, 1990–2000. IEEE Geosci. Remote Sens. Lett. 3, 68–72.

Meng, W., Feagin, R.A., Innocenti, R.A., Hu, B., He, M., Li, H., 2020. Invasion and ecological effects of exotic smooth cordgrass Spartina alterniflora in China. Ecol. Eng. 143, 105670.

Ren, G., Zhao, Y., Wang, J., Wu, P., Ma, Y., 2021a. Ecological effects analysis of Spartina alterniflora invasion within Yellow River delta using long time series remote sensing imagery. Estuar. Coast. Shelf Sci. 249, 107111.

Ren, J., Chen, J., Xu, C., Koppel, J.v.d., Thomsen, M.S., Qiu, S., Cheng, F., Song, W., Liu, Q.-X., Xu, C., Bai, J., Zhang, Y., Cui, B., Bertness, M.D., Silliman, B.R., Li, B., He, Q., 2021b. An invasive species erodes the performance of coastal wetland protected areas. Science Advances 7, eabi8943.

Sun, C., Li, J., Liu, Y., Liu, Y., Liu, R., 2021. Plant species classification in salt marshes using phenological parameters derived from Sentinel-2 pixel-differential time-series. Remote Sens. Environ. 256, 112320.

Sun, C., Liu, Y., Zhao, S., Zhou, M., Yang, Y., Li, F., 2016. Classification mapping and species identification of salt marshes based on a short-time interval NDVI time-series from HJ-1 optical imagery. Int. J. Appl. Earth Obs. 45, 27–41.

Tucker, C.J., 1979. Red and photographic infrared linear combinations fro monitoring vegetation. Remote Sens. Environ. 8, 127–150.

Vaz, A.S., Alcaraz-Segura, D., Campos, J.C., Vicente, J.R., Honrado, J.P., 2018. Managing plant invasions through the lens of remote sensing: a review of progress and the way forward. Sci. Total Environ. 642, 1328–1339.
Vermote, E., Justice, C., Claverie, M., Franch, B., 2016. Preliminary analysis of the performance of the Landsat 8/OLI land surface reflectance product. Remote Sens. Environ. 185, 46–56.
Wang, X., Wang, L., Tian, J., Shi, C., 2021a. Object-based spectral-phenological features for mapping invasive Spartina alterniflora. Int. J. Appl. Earth Obs. 101, 102349.
Wang, X., Xiao, X., Xu, X., Zou, Z., Chen, B., Qin, Y., Zhang, X., Dong, J., Liu, D., Pan, L., Li, B., 2021b. Rebound in China's coastal wetlands following conservation and restoration. Nat. Sustain. 4, 1076–1083.
Wang, X., Xiao, X., Zou, Z., Chen, B., Ma, J., Dong, J., Doughty, R.B., Zhong, Q., Qin, Y., Dai, S., Li, X., Zhao, B., Li, B., 2018. Tracking annual changes of coastal tidal flats in China during 1986–2016 through analyses of Landsat images with Google Earth Engine. Remote Sens. Environ. 238, 110987.
Wang, X., Xiao, X., Zou, Z., Hou, L., Qin, Y., Dong, J., Doughty, R.B., Chen, B., Zhang, X., Chen, Y., Ma, J., Zhao, B., Li, B., 2020. Mapping coastal wetlands of China using time series Landsat images in 2018 and Google Earth Engine. ISPRS J. Photogramm. Remote Sens. 163, 312–326.
Xiao, X., Biradar, C., Czarnecki, C., Alabi, T., Keller, M., 2009. A Simple Algorithm for Large-Scale Mapping of Evergreen Forests in Tropical America, Africa and Asia. Remote Sens. 1, 355–374.
Xiao, X., Boles, S., Liu, J., Zhuang, D., Frolking, S., Li, C., Salas, W., Moore, B., 2005. Mapping paddy rice agriculture in southern China using multi-temporal MODIS images. Remote Sens. Environ. 95, 480–492.
Xie, R., Zhu, Y., Li, J., Liang, Q., 2019. Changes in sediment nutrients following Spartina alterniflora invasion in a subtropical estuarine wetland, China. Catena 180, 16–23.
Xie, T., Wang, Q., Ning, Z., Chen, C., Cui, B., Bai, J., Shi, W., Pang, B., 2021. Artificial modification on lateral hydrological connectivity promotes range expansion of invasive Spartina alterniflora in salt marshes of the Yellow River delta. China. Sci. Total Environ. 769, 144476.
Xu, H., 2006. Modification of normalised difference water index (NDWI) to enhance open water features in remotely sensed imagery. Int. J. Remote Sens. 27, 3025–3033.
Yan, D., Li, J., Yao, X., Luan, Z., 2021. Quantifying the long-term expansion and dieback of Spartina Alterniflora using google earth engine and object-based hierarchical random forest classification. IEEE J Sel. Top. Appl. Earth Observ. Remote Sens. 14, 9781–9793.
Yuan, L., Zhang, L., Xiao, D., Huang, H., 2011. The application of cutting plus waterlogging to control Spartina alterniflora on saltmarshes in the Yangtze Estuary. China. Estuar. Coast. Shelf Sci. 92, 103–110.
Zeng, J., Sun, Y., Cao, P., Wang, H., 2022. A phenology-based vegetation index classification (PVC) algorithm for coastal salt marshes using Landsat 8 images. Int. J. Appl. Earth Obs. 110, 102776.
Zhang, D., Hu, Y., Liu, M., Chang, Y., Sun, L., 2020a. Geographical variation and influencing factors of Spartina alterniflora expansion rate in Coastal China. Chin. Geogr. Sci. 30, 127–141.
Zhang, D., Hu, Y., Liu, M., Chang, Y., Yan, X., Bu, R., Zhao, D., Li, Z., 2017. Introduction and Spread of an Exotic Plant, Spartina alterniflora, Along Coastal Marshes of China. Wetlands 37, 1181–1193.
Zhang, X., Friedl, M.A., Schaaf, C.B., Strahler, A.H., Hodges, J.C.F., Gao, F., Reed, B.C., Huete, A., 2003. Monitoring vegetation phenology using MODIS. Remote Sens. Environ. 84, 471–475.
Zhang, X., Xiao, X., Qiu, S., Xu, X., Wang, X., Chang, Q., Wu, J., Li, B., 2022. Quantifying latitudinal variation in land surface phenology of Spartina alterniflora saltmarshes across coastal wetlands in China by Landsat 7/8 and Sentinel-2 images. Remote Sens. Environ. 269, 112810.
Zhang, X., Xiao, X., Wang, X., Xu, X., Chen, B., Wang, J., Ma, J., Zhao, B., Li, B., 2020b. Quantifying expansion and removal of Spartina alterniflora on Chongming island, China, using time series Landsat images during 1995–2018. Remote Sens. Environ. 247, 111916.
Zhao, Z., Xu, Y., Yuan, L., Li, W., Zhu, X., Zhang, L., 2020. Emergency control of Spartina alterniflora re-invasion with a chemical method in Chongming Dongtan, China. Water Sci. Eng. 13, 24–33.
Zhou, Y., Dong, J., Xiao, X., Xiao, T., Yang, Z., Zhao, G., Zou, Z., Qin, Y., 2017. Open surface water mapping algorithms: a comparison of water-related spectral indices and sensors. Water 9.
Zhu, W., Ren, G., Wang, J., Wang, J., Hu, Y., Lin, Z., Li, W., Zhao, Y., Li, S., Wang, N., 2022. Monitoring the invasive plant spartina alterniflora in Jiangsu Coastal Wetland Using MRCNN and long-time series landsat data. Remote Sens. 14, 2630.
Zhu, X., Meng, L., Zhang, Y., Weng, Q., Morris, J., 2019. Tidal and meteorological influences on the growth of invasive Spartina alterniflora: evidence from UAV remote sensing. Remote Sens. 11, 1208.
Zhu, Z., Woodcock, C.E., 2012. Object-based cloud and cloud shadow detection in Landsat imagery. Remote Sens. Environ. 118, 83–94.
Zuo, P., Zhao, S., Liu, C., Wang, C., Liang, Y., 2012. Distribution of Spartina spp. along China's coast. Ecol. Eng. 40, 160–166.